


Vibration signatures of the structural phase transition of Sn/Ge(111) compared to Sn/Si(111)B. Halbig,^{*} U. Bass, and J. Geurts*Universität Würzburg, Physikalisches Institut, Experimentelle Physik 3, Am Hubland, 97074 Würzburg, Germany*

S. Sanna

*Justus-Liebig-Universität Gießen, Institut für Theoretische Physik and Center for Materials Research (LaMa),
Heinrich-Buff-Ring 16, 35392 Gießen, Germany* (Received 1 October 2018; revised manuscript received 2 July 2019; published 26 July 2019)

A temperature driven structural phase transition between $(\sqrt{3}\times\sqrt{3})$ and (3×3) has been reported for Sn adsorbed on the Ge(111) surface, which does not occur for the analogous Sn/Si(111) system. This phase transition has been correlated to a softening of a low-frequency Sn vibration mode, referred to as dynamical fluctuation mode. We have determined the eigenfrequencies of the vibration modes of Sn/Ge(111) and Sn/Si(111) with high accuracy by *in situ* surface Raman spectroscopy in the temperature range between 300 and 40 K, and calculated the surface reconstructions and vibration eigenmodes by density functional theory. Our calculated vibration eigenfrequencies are in excellent agreement with the observed Raman peak positions and the calculated displacement patterns allow the assignment of all observed vibration modes. Our results for both adsorbate systems Sn/Ge(111) and Sn/Si(111) show the preservation of the global surface atom configuration over the whole investigated temperature range. The emergence of a backfolded Rayleigh wave at $\approx 50\text{ cm}^{-1}$ for Sn/Ge(111) below $\approx 200\text{ K}$ is a clear signature of its transition to a static (3×3) reconstruction. The gradual intensity increase of this mode upon further cooling suggests an order-disorder character of this transition.

DOI: [10.1103/PhysRevB.100.035437](https://doi.org/10.1103/PhysRevB.100.035437)**I. INTRODUCTION**

The atomic arrangement as well as the electronic and vibration properties of semiconductor surfaces may substantially differ from their bulk counterpart. Reconstructed surfaces therefore show novel physical effects connected to the reduced dimensionality. The (111)-oriented clean surfaces of the well-known semiconductors Ge and Si reconstruct as Ge(111)- $c(2\times 8)$ and Si(111)- (7×7) [1,2]. These surfaces are very suitable as substrates for self-ordered arrangements of metal adatoms (e.g., Sn, Au, etc.), which show various manifestations of many-body physics due to electronic correlations [3,4].

The Ge(111)- $c(2\times 8)$ reconstruction is of special interest, both intrinsically as well as as a pre-stage for the adatom system Sn/Ge(111). Compared to the unreconstructed Ge(111) surface, the Ge(111)- $c(2\times 8)$ reconstruction has two additional Ge adatoms per primitive surface unit cell. The adatoms occupy T_4 positions with three next neighbors in the first layer of bulk-like Ge(111) and one Ge atom vertically underneath in the second layer [5,6]. Furthermore, two atoms of the first layer, called restatoms, are shifted upwards to minimize the surface energy [7]. Static displacements of atomic positions due to the ad- and restatoms on the surface reach several layers deep into the bulk. The Ge(111)- $c(2\times 8)$ reconstruction has no point symmetry properties. In particular, there are no mirror planes, as the adatoms and restatoms are not equivalent [8,9]. In addition to the atomic structure, surface dynamics and

phonons were analyzed theoretically [7] and several vibration modes were identified by inelastic He atom scattering (HAS) [10].

A self-ordered adsorbate structure with a reported periodicity of $(\sqrt{3}\times\sqrt{3})$ at 300 K [11,12] is formed upon adsorption of $1/3$ monolayer (ML) of Sn on the Ge(111) surface. The same applies for the adsorption of Sn on Si(111) [13]. In spite of this similarity at room temperature, crucial differences have been reported at low temperature. For Sn/Ge(111), a reversible structural phase transition (SPT) from $(\sqrt{3}\times\sqrt{3})$ to (3×3) occurs upon cooling at $T_{\text{SPT}} \approx 210\text{--}220\text{ K}$, as shown by scanning tunneling microscopy (STM) and HAS measurements [12,14]. The atomic structure of Sn/Ge(111) with indicated reconstruction unit cells is shown in Fig. 1. In contrast, for Sn/Si(111) the $(\sqrt{3}\times\sqrt{3})$ reconstruction persists at low temperatures, as indicated by STM measurements [13]. Apart from the absence of the structural phase transition, other interesting effects were reported for Sn/Si(111). A Mott transition to an insulating ground state was observed below 60 K [15]. Also for Sn/Ge(111), a Mott insulating ground state, accompanied by the return to the $(\sqrt{3}\times\sqrt{3})$ reconstruction, was found below 30 K [16]. For both systems, this Mott behavior was also revealed in *ab initio* calculations [17]. Furthermore, in a combined theoretical and experimental study, a row-wise antiferromagnetic spin alignment of the Sn atoms in the triangular lattice of Sn- $(\sqrt{3}\times\sqrt{3})$ /Si(111) was reported [18].

To explain this different structural behavior of Sn/Ge(111) and Sn/Si(111), several models were proposed, including the charge density wave model [12,19,20], defect-related models

^{*}benedikt.halbig@physik.uni-wuerzburg.de

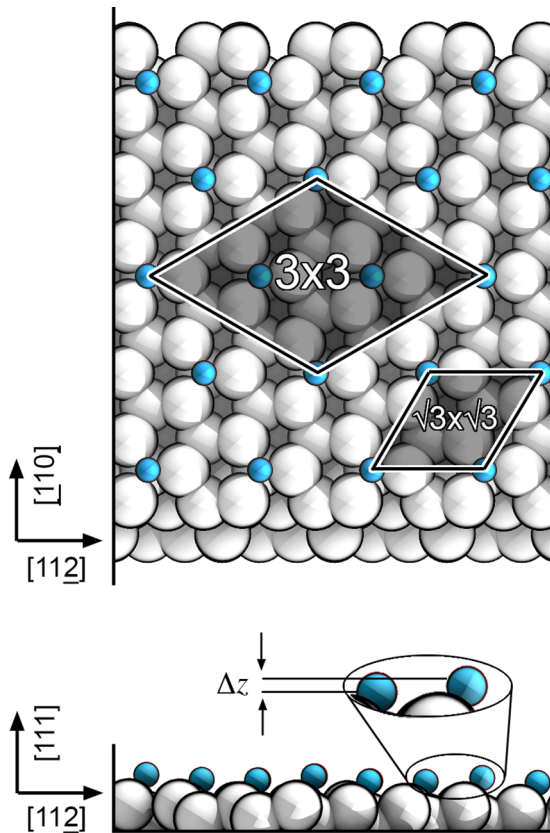


FIG. 1. Model of the atomic structure of the Sn-(3×3)/Ge(111) reconstruction (top view on the top and side view in $\bar{1}10$ direction at the bottom). The Sn atoms are shown as blue spheres (not in scale). The protruding ones on “up” positions induce the (3×3) periodicity. Disregard of the height differences results in the $(\sqrt{3}\times\sqrt{3})R30^\circ$ reconstruction.

[21,22], and the dynamical fluctuation (DF) model [23–26]. The latter is illustrated by the atomic structure and the corresponding surface unit cells shown in Fig. 1. If all Sn atoms on the T_4 positions lay at the same height, the reconstruction has the $(\sqrt{3}\times\sqrt{3})R30^\circ$ periodicity. However, structural analysis by x-ray standing wave measurements has shown that not all Sn atoms are equivalent. Every third Sn atom along the $[11\bar{2}]$ direction shows a slight upward displacement (“up” position), while two Sn atoms are at a lower height (“down” position) [27]. This configuration results in a (3×3) surface unit cell. The height difference between the upper Sn atom and the two lower ones is $\Delta z = 0.3\text{--}0.45 \text{ \AA}$ [27,28]. According to a time-resolved STM study, the “up” atom exchanges its vertical position with the “down” atoms on a time scale of 1 ms at 220 K [26], while calculations suggest a much shorter time scale [29]. The time average of the fluctuations results in a $(\sqrt{3}\times\sqrt{3})$ reconstruction, as observed, e.g., in low-energy electron diffraction (LEED) and conventional STM at room temperature [12]. When the temperature is below T_{SPT} , the Sn atoms freeze into a long-range configuration leading to a (3×3) pattern, i.e., a reversible $(\sqrt{3}\times\sqrt{3}) \leftrightarrow (3\times 3)$ phase transition occurs. Within the DF model, this transition was proposed to be mediated by a soft phonon mode [24], denoted as DF mode. At high temperatures, e.g., 300 K, the dynamic processes at the surfaces of Sn/Ge(111) and Sn/Si(111) are

predicted to be likewise described by the DF model [24, 30–32]. To verify this model, a profound knowledge of the dynamic characteristics of the surface is necessary. For Sn/Ge(111), calculations and HAS experiments, have been performed to reveal the surface phonon properties [24,29,33]. For Sn/Si(111) no experimental results on surface vibrations are available.

The experimental analysis of adatom-induced surface vibration eigenmodes together with theoretical modeling already has offered valuable insight for several material systems [34–37], as the vibration eigenfrequencies and symmetry properties are determined by the atomic positions and bond orbitals. For Sn/Ge(111) and Sn/Si(111), the vibration mode analysis should, beside this general aspect, have an additional relevance, as the lattice dynamics has been predicted to play a key role in the structural phase transition [24].

A well suited method for surface vibration analysis is surface Raman spectroscopy (SRS). Its eligibility regarding sensitivity and nondestructiveness was demonstrated, e.g., for Ge(001)- $p(2\times 1)/c(4\times 2)$, Si(111)- (7×7) , and Au- $(\sqrt{3}\times\sqrt{3})/\text{Si}(111)$. For these systems, the analysis of the atomic structure as well as the identification of specific vibration patterns in combination with calculations were reported [38–40]. A significant merit of SRS is the very high spectral resolution in the range of 1 cm^{-1} , which is superior to, e.g., HAS. An energy resolution of $\approx 3 \text{ cm}^{-1}$ is stated for the HAS measurements reported here [10,29,41].

In this work, we present an *in situ* Raman investigation of the temperature dependence and symmetry of the vibration eigenmodes of Sn/Ge(111) and the related system Sn/Si(111). Corresponding density functional theory (DFT) calculations are performed to assign vibration patterns to the measured Raman features, and thus provide an interpretation of the experimental spectral signatures. Evidence for the structural phase transition of Sn/Ge(111) at low temperatures is observed and interpreted within the dynamical fluctuation model. A clearly different temperature behavior is found for the Sn/Si(111) counterpart. As expected, here no structural transition is observed.

II. METHODOLOGY

A. Experimental details

Sample preparation and Raman measurements were conducted *in situ* in an ultrahigh-vacuum (UHV) chamber (base pressure $p < 1\times 10^{-10}$ mbar) to prevent the surface from contamination. For preparation, polished doped substrates of Ge(111) (p -type, dopant B, $\rho = 0.05\text{--}1.3 \text{ \Omega cm}$) and Si(111) (n -type, dopant P, $\rho = 0.009\text{--}0.011 \text{ \Omega cm}$) were used. After *ex situ* cleaning by subsequent boiling in acetone and methanol, the substrates were degassed *in situ* at $\approx 900 \text{ K}$ for several hours by direct current heating. The Ge(111) samples were prepared by several cycles of sputtering with Ar^+ ions at $E = 1 \text{ keV}$ ($p \approx 1\text{--}2\times 10^{-6}$ mbar) and subsequent annealing at 1100 K. The temperature was monitored by a pyrometer. The quality of the clean surface reconstruction Ge(111)- $c(2\times 8)$ was assured by LEED. The Si(111) samples were prepared by flash-annealing cycles at 1550 K to obtain the clean Si(111)- (7×7) surface reconstruction. Details of this

preparation procedure are published elsewhere [40]. Onto the clean surfaces, 1/3 ML of Sn was deposited by an e-beam evaporator and surveyed by a quartz crystal microbalance. After Sn deposition, the samples were annealed for ≈ 3 min at ≈ 560 K for Ge(111) and ≈ 970 K for Si(111). Finally, the desired surface reconstruction and its quality were affirmed by LEED.

Raman analyses were performed at room temperature (RT) and in the low temperature range between 200 and ≈ 40 K (denoted as LT) obtained with a continuous-flow He cryostat. Measurements at LT were well below T_{SPT} of the Sn/Ge(111) transition from $(\sqrt{3} \times \sqrt{3})$ to (3×3) , but above the transition temperature to the low-temperature $(\sqrt{3} \times \sqrt{3})$ reconstruction.

The laser lines 488 nm (≈ 2.54 eV) and 514 nm (≈ 2.41 eV) of an Ar⁺ ion laser were used to excite the samples. The laser power was in the range of 100–300 mW. The Raman scattered light was analyzed by a single grating monochromator (SPEX 1000M) equipped with a Si-based CCD detector (ANDOR iDUS series). Depending on the intensity of the elastically scattered laser light, it was blocked either by an edge filter (SEMROCK Razor Edge) or by two Bragg notch filters (OPTIGRATE BragGrate) in order to approach the laser line as close as possible. The edge filter allowed measurements as close as 35 cm^{-1} to the laser line, while the Bragg notch filters enable Stokes and anti-Stokes spectra down to 25 cm^{-1} . Typical integration times for a single Raman spectrum are 900 s. The spectral peak position accuracy is $\approx 0.1 \text{ cm}^{-1}$. All Raman spectra which are shown here are recorded with the 488-nm laser line, but our results were reproduced and verified with the 514-nm laser line.

The Raman spectra were recorded in quasibackscattering geometry in different polarization configurations, which are denoted according to the Porto notation [42,43]. For an incident beam normal to the (111)-oriented surface (defined as z direction) and polarized according to $x \parallel [11\bar{2}]$, there are two possible configurations. The scattered light is analyzed either in x or y polarization, with $y \parallel [\bar{1}10]$. The spectra are therefore denoted as $z(xx)\bar{z}$ and $z(xy)\bar{z}$. A $\lambda/2$ plate is used to exploit for both polarization configurations the same efficiency of the monochromator grating.

B. Computational details

The investigated surfaces are modeled with asymmetric slabs, which include six Si or Ge bilayers stacked along the [111] crystallographic direction to model the substrate, the Sn surface termination, and a vacuum region of about 20 \AA . H atoms saturate the dangling bonds at the backside face of the slabs. Surfaces with $(\sqrt{3} \times \sqrt{3})$ periodicity are thus modeled by slabs of 40 atoms, while 120 atom cells are necessary to model surfaces with (3×3) periodicity. The atomic positions are optimized until the residual Hellmann-Feynman forces are below 0.001 eV/\AA . Three Si(Ge) bilayers and the H atoms are kept at their bulk positions in order to model the substrate, while the Sn layer and the remaining Si(Ge) atoms are allowed to relax. Dipole corrections [44,45] are employed to account for the artificial electric field created by the slab images on both electronic structure and equilibrium geometry.

For the modeling of the structural and vibration properties of both material systems the DFT is employed,

as implemented in the Vienna ab initio simulation package (VASP) [46,47]. In order to estimate the influence of the exchange-correlation functional on our results, total-energy and frozen-phonon calculations [48] are performed both within the local density approximation (LDA) [49,50] and within the generalized gradient approximation (GGA) in the Perdew-Burke-Ernzerhof (PBE) formulation [51,52]. Projector augmented wave (PAW) potentials [53,54] with projectors up to $l = 1$ for H and $l = 2$ for Si, Ge, and Sn are used. Four valence electrons were employed for the simulation of the Si ($3s^2 3p^2$), Ge ($4s^2 4p^2$), and Sn ($5s^2 5p^2$), while a single valence electron ($1s^1$) is considered for H. The electronic wave functions are expanded into plane waves up to an energy cutoff of 400 eV.

A $12 \times 12 \times 1$ Monkhorst-Pack [55] k -point mesh is used to perform the integration in the Brillouin zone (BZ) of the cells with $(\sqrt{3} \times \sqrt{3})$ periodicity, while a $6 \times 6 \times 1$ mesh is employed for cells of (3×3) periodicity. The convergence of the phonon eigenvalues with respect to the number of mobile atomic layers is tested. The calculated phonon eigenfrequencies depend to some extent on the details of the calculations, such as the exchange-correlation functional or the substrate lattice constant. For our calculations of the phonon modes both with LDA and GGA, we have employed the Si(Ge) experimental lattice constant. We show in this work the values calculated within DFT-LDA, as the frequencies calculated with DFT-GGA agree for most phonons within few cm^{-1} . The largest calculated deviation between DFT-LDA and DFT-GGA amounts to 13 cm^{-1} , which is considered as an upper bound for the uncertainty of our approach.

III. RESULTS AND DISCUSSION

Firstly, in Sec. III A, Raman spectra of the clean Ge(111)- $c(2 \times 8)$ are surveyed (i) as a reference for Sn/Ge(111) and (ii) as an illustration for our procedure to deduce the net contribution of the surface phonon modes from the pristine Raman spectrum. Raman reference data from the clean Si(111)- (7×7) surface are omitted, since they have been presented in Ref. [39]. Subsequently, the adsorbate systems Sn/Ge(111) and Sn/Si(111) are examined. Section III B covers the calculated structural properties of both systems, while the surface vibration results from experiment and calculations in the higher frequency range are presented for Sn/Si(111) in Sec. III C and for Sn/Ge(111) in Sec. III D. Finally, the low-frequency modes of both systems, which are relevant for the discussion of the structural phase transition, are evaluated and compared in Sec. III E.

A. Vibration modes of Ge(111)- $c(2 \times 8)$

Figure 2 shows Raman spectra of Ge(111)- $c(2 \times 8)$ and unreconstructed Ge(111) for comparison. As unreconstructed surface, either an aged and degraded reconstructed surface or an unprepared surface was used. The spectral intensity difference between Ge(111)- $c(2 \times 8)$ and unreconstructed Ge(111) is marked by a grey shading. Its spectral features are attributed to the reconstruction-induced surface vibration modes and in the following the shaded area is denoted as surface Raman spectrum. In all pristine spectra, the main contributions

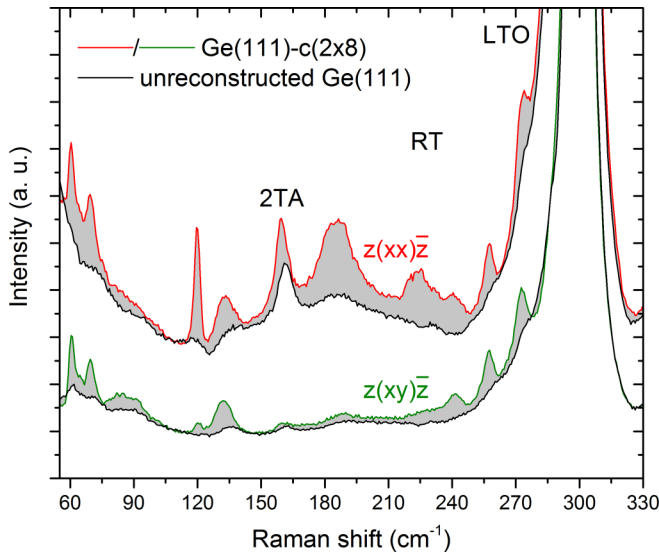


FIG. 2. Polarized Raman spectra at room temperature (RT) of the Ge(111)-c(2×8) reconstruction for the polarization configurations $z(xx)\bar{z}$ (red) and $z(xy)\bar{z}$ (green) and the unreconstructed surface (black). For the c(2×8) reconstruction, additional features arise (shaded area) which are assigned to reconstruction-induced surface vibration modes.

originate from the bulk. The dominant peak is the degenerate longitudinal and transversal optical (LTO) phonon located at 300 cm^{-1} . This peak is about a factor 10^2 more intense than the other structures. It is strongly cropped to visualize the surface vibrations in greater detail. Furthermore, the surface vibration peaks are superimposed on a broad structured background due to second-order scattering from bulk modes [56].

The surface Raman spectra of Ge(111)-c(2×8) at LT ($\approx 40\text{ K}$) are depicted in Fig. 3. They provide more detailed information than the RT spectra, as narrower peaks and eventually finer structures become visible. The peak frequencies

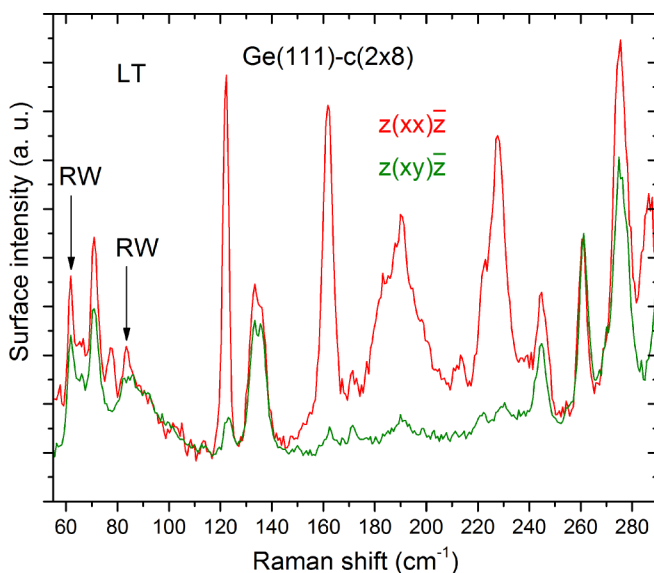


FIG. 3. Polarized surface Raman spectra of Ge(111)-c(2×8) at low temperature (LT, $\approx 40\text{ K}$). The labels “RW” indicate backfolded Rayleigh waves.

TABLE I. Vibration peak frequencies (in cm^{-1}) of Ge(111)-c(2×8) in $z(xx)\bar{z}$ configuration. Surface Raman spectroscopy (SRS) data are presented for room temperature (RT) and low temperature (LT, $\approx 40\text{ K}$). Results from molecular dynamics simulations (MD) [7] and experimental ones from He atom scattering (HAS) [10] are listed for comparison. The results of the calculations are indexed as vibration contributions from the adatoms (AA) and from the restatoms and atoms in the first complete layer (RA). The backfolded Rayleigh waves (RWs) types, obtained from HAS, are indicated in the last column.

SRS		MD		HAS	type
RT	LT	AA	RA		
				35	
				44	
60.2	61.6	62	62	64	RW
64.4	64.9				
69.7	69.9	76	74	78	
74.5	77.3				
88.2	83.6		101	89	RW
119.7	121.7	122		120	
131.7	132.1				
135.6	135.4	135			
159.4	161.3	152		159	
	171.5				
181.7	182.4				
187.9	189.7		189	186	
	211.9				
219.3	221.5		221		
224.8	227.6				
239.5	244.1				
257.1	260.2				
272.3	274.8		276		
282.9	285.7				

for RT and LT are listed in Table I together with eigenfrequencies, obtained from a molecular dynamics simulation (MD) [7] and HAS, giving altogether a consistent picture. Note, however, that the Raman data yield a considerably enhanced frequency accuracy compared to HAS, which could not resolve frequency shifts between RT and 170 K. Moreover, the Raman data allow the identification of several vibration modes which did not occur in HAS. According to the MD study, most of the vibration mode peaks can be attributed to the Ge adatoms or to the restatoms and other atoms in the same layer.

The most prominent feature in the surface Raman spectra of Ge(111)-c(2×8) at LT is a very narrow peak at 121.7 cm^{-1} . According to HAS, this peak belongs to an optical surface phonon with a flat dispersion [10], which is attributed to the adatoms. Furthermore, distinct optical surface phonons are observed, e.g., at 161.3 and 189.7 cm^{-1} . In the upper frequency region, at the edge of the bulk Ge LTO phonon, there are three peaks above $\approx 250\text{ cm}^{-1}$, which might result from backfolding of the LO and TO branch at the surface with respect to the bulk phonon dispersion [57,58].

In the low-frequency range, in accordance with HAS [10], the spectral features at 61.6 and 83.6 cm^{-1} are assigned to Rayleigh waves (RWs), i.e., acoustic-phonon-like

TABLE II. Si(Ge)-Sn bond lengths calculated within LDA and GGA for the Sn/Si(Ge)(111)-($\sqrt{3}\times\sqrt{3}$) system. All lengths are in angstroms.

	LDA	GGA
Si-Sn	2.754	2.789
Ge-Sn	2.796	2.844

near-surface waves with reduced phase velocity, which decay exponentially into the bulk [59]. The observed eigenfrequencies originate from eigenvalues at Brillouin-zone edges, which are backfolded due to the surface reconstruction and therefore become accessible for SRS. The high-intensity Raman peak at 69.9 cm^{-1} is identified with a HAS feature observed between the RWs.

Overall, our Raman results show a very good consistency with MD calculations and offer a distinct experimental refinement with respect to previous HAS data.

B. Structure of Sn/Si(111) and Sn/Ge(111)

As a first step of the investigation of the Sn/Si(Ge)(111) system, we model the structural properties of the ($\sqrt{3}\times\sqrt{3}$) reconstructions. Within this reconstruction, the Sn atoms occupy the T_4 positions, both on Si and Ge substrates. They form three equivalent bonds with the first Si(Ge) neighbors. The calculated bond lengths are shown in Table II. Both DFT-LDA and DFT-GGA predict for either system bond lengths of $\approx 2.7\text{--}2.8\text{ \AA}$, although as expected LDA tends to overestimate the bond strength and underestimate the bond distances. The calculated distances are slightly longer than the sum of the atom's covalent radii, which is 2.52 \AA for Si-Sn and 2.63 \AA for Ge-Sn [60]. A corresponding contour plot of the electronic charge density in a plane containing the Si(Ge)-Sn bond is shown in Fig. 4. Very similar charge distributions are predicted for both systems, with some charge accumulation between Si(Ge) and Sn. Bond distances and charge distributions suggest that Sn forms a covalent bond with the Si(Ge) atoms, although less strong than the homoatomic Si-Si or Ge-Ge bond.

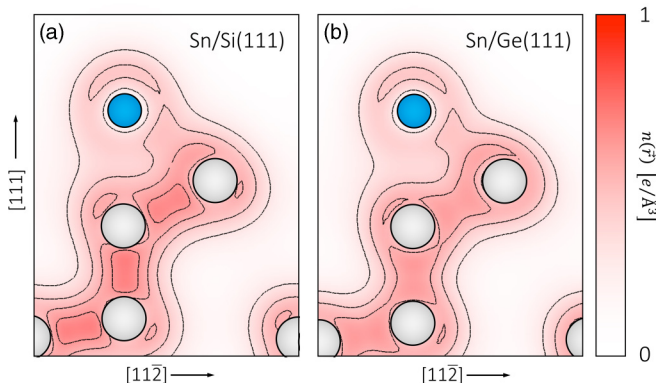


FIG. 4. Contour plot of the electronic charge density of Sn-($\sqrt{3}\times\sqrt{3}$)/Si(111) (a) and Sn-($\sqrt{3}\times\sqrt{3}$)/Ge(111) (b), calculated within DFT-LDA in the (110) crystallographic plane containing one of the three equivalent Sn-Si(Ge) bonds.

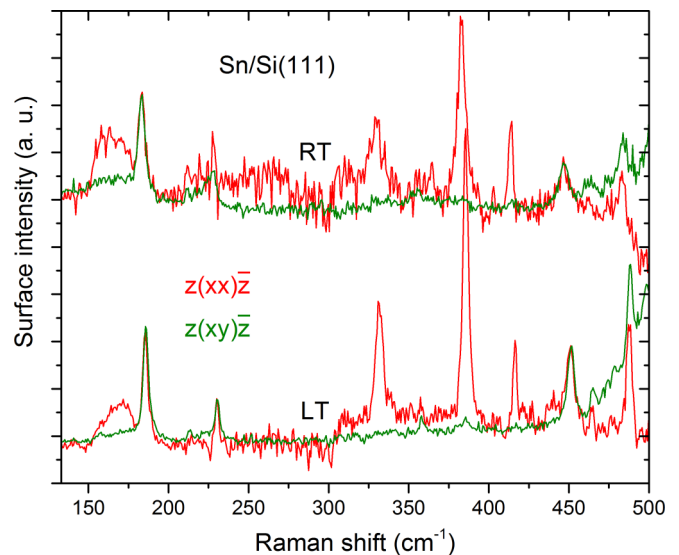


FIG. 5. Surface Raman spectra of the Sn/Si(111) surface at room temperature (RT) and at low temperature (LT, $\approx 40\text{ K}$) for $z(xx)\bar{z}$ and $z(xy)\bar{z}$ polarization configurations in the frequency range from 130 to 500 cm^{-1} . The range below 130 cm^{-1} is covered in Sec. III E.

If a (3×3) periodicity is allowed in the calculation, the Sn atoms still occupy the T_4 positions on both substrates. However, while on Si(111) the final positions of the Sn atoms are the same as in the ($\sqrt{3}\times\sqrt{3}$) reconstruction, the Sn atoms on Ge(111) are at different heights after relaxation. Structural optimization within different starting configurations shows that Sn adsorption with and without vertical distortion are global minima of the configuration space for Ge(111) and Si(111), respectively. The Sn height difference for Sn/Ge(111) is estimated in about 0.3 \AA both in DFT-LDA and DFT-GGA.

C. High-frequency vibration modes of Sn/Si(111)

When the clean Si(111)-(7×7) surface is covered with $1/3$ ML of Sn, the Sn atoms lead to a new surface reconstruction. The LEED pattern of the Sn/Si(111) system clearly shows the formation of a ($\sqrt{3}\times\sqrt{3}$) periodicity. The pattern is rotated by 30° with respect to the (1×1) of the Ge(111) substrate, as an evidence for a ($\sqrt{3}\times\sqrt{3}$) $R30^\circ$ reconstruction. This reconstruction belongs to the space group $p31m$, also associated with the point group C_{3v} [61]. It contains Raman-active A-like and E-like vibration modes. In the bulk, Raman-active A modes have A_1 symmetry. A_2 modes, normally silent, can become Raman active at the surface. According to group theory, the A modes appear in the polarization configuration $z(xx)\bar{z}$, whereas the E modes appear in $z(xx)\bar{z}$ and $z(xy)\bar{z}$ [43].

In the calculations, phonon modes can be divided into A modes, which are nondegenerate and preserve the threefold rotational symmetry, and E modes, which are twofold degenerate and reduce the crystal symmetry. Furthermore, we only consider surface localized modes, which have a fraction $>25\%$ of the atomic displacement localized within the top-most three atomic layers.

The surface Raman spectra of Sn/Si(111) for RT and LT are shown in Fig. 5 and the peak frequencies are listed in Table III, together with calculated vibration frequencies.

TABLE III. Vibration peak frequencies (in cm^{-1}) of Sn/Si(111) above $\approx 130 \text{ cm}^{-1}$ measured by Surface Raman spectroscopy (SRS) in $z(xx)\bar{z}$ polarization configuration. Data are presented for room temperature (RT) and low temperature (LT, $\approx 40 \text{ K}$) and compared with values calculated within DFT-LDA.

SRS			DFT	
Sym.	RT	LT	Sym.	LDA
			A	146.1
A	164.6	169.4	A	161.3
E	183.4	185.5	E	174.9
E	227.8	230.3	E	219.3
A	212.4	214.8	A	222.7
A	308.6	309.8	A	308.0
A			A	311.2
A	329.5	331.9	A	329.5
E	350.0	350.4	E	347.3
A	356.7	358.2	A	352.7
A	383.0	385.5	A	380.9
A	413.7	416.5	A	421.3
E	447.1	450.5	E	437.0
E	482.9	487.5	E	474.9
			A	505.0

The Sn adsorption has quenched the typical Raman features of the clean Si(111)- (7×7) , which we have presented and discussed in detail elsewhere [39]. Instead, different features are observed between 150 and 500 cm^{-1} , the most relevant ones being located at about 180 and 380 cm^{-1} . In the covered frequency range, our atomistic calculations reveal the presence of 14 surface localized modes. These correspond to the measured Raman features and yield valuable information for the interpretation of the measured spectra. All the measured features are predicted by the calculations, which reproduce the experimental RT (LT) results with an average deviation of 5.5 (7.2) cm^{-1} . The mode assignment, symmetry, and displacement patterns are discussed in the following.

In the LT spectra, at 185.5 cm^{-1} , there is a distinct eigenmode with a low-frequency shoulder. This peak is observed in both polarization configurations, suggesting that it is an E mode. The shoulder peak, centered at 169.4 cm^{-1} has A symmetry. Accordingly, our calculations yield an A mode at 161.3 cm^{-1} [see Fig. 6(a)], which is a vertical displacement in antiphase of Sn and of the lower lying Si dimer, which moves rigidly. This mode features a substantial Sn involvement, which explains its low frequency. The eigenvector of the E mode at 185.5 cm^{-1} is a tilting of the Si trimer bound to the Sn atom as shown in Fig. 6(b).

At approximately 223 cm^{-1} calculations predict a surface localized mode that can be spotted as a very low intensity feature at about 215 cm^{-1} in the measured LT spectra. Its eigenvector is depicted in Fig. 6(c), and represents an antiphase movement of the first and third Si double layer without Sn participation. Due to its symmetry this mode is not expected to drastically modify the lattice polarizability, which explains its low Raman cross section.

The E-symmetry peak at 230.3 cm^{-1} is linked to a calculated mode at 219.3 cm^{-1} with a rather complex eigenvector.

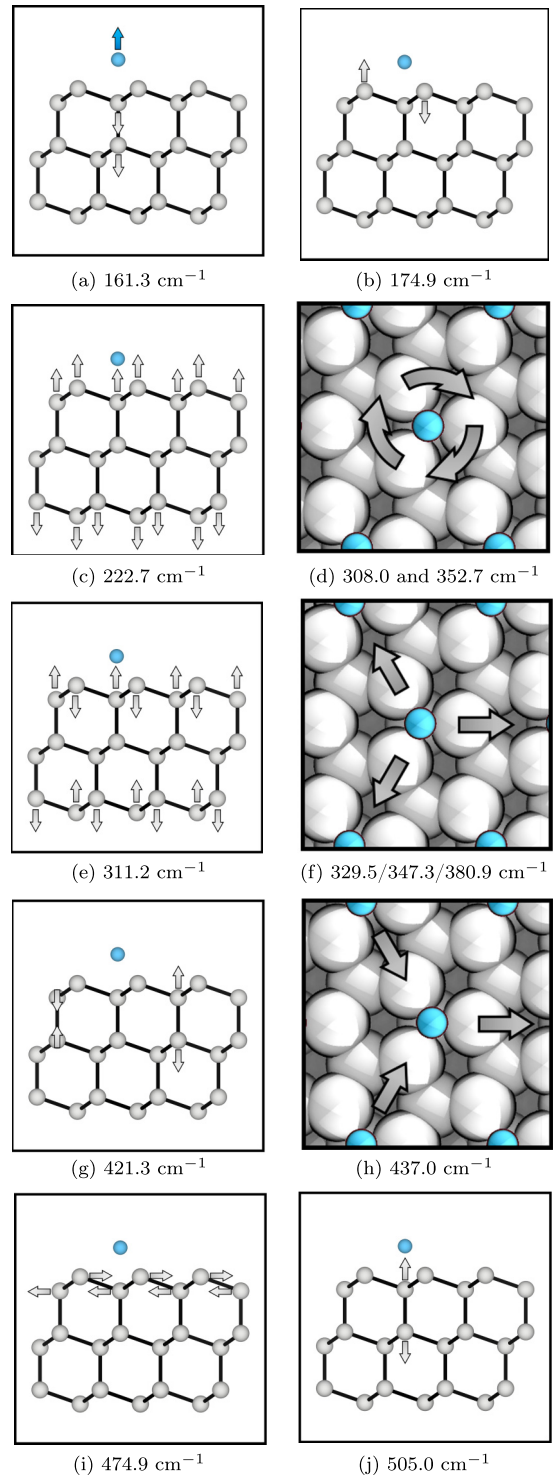


FIG. 6. Calculated displacement pattern and eigenfrequency of selected surface localized phonon modes in the Sn- $(\sqrt{3}\times\sqrt{3})$ /Si(111) system. The arrows show the atomic displacement within the $(\sqrt{3}\times\sqrt{3})$ surface unit cell. The double and triple frequency values in panels (d) and (f) correspond to different participation of underlying Si layers.

One of the three Si atoms bound to Sn moves towards the Sn atom in the bond direction. In turn, it causes the distortion of the neighboring Si trimer.

The step-like structure at 300–310 cm^{-1} appears because of reconstruction-induced changes in the edge of the 2TA phonon. The two peaks of A symmetry predicted by theory in this region (308.0 and 311.2 cm^{-1}) are thus difficult to observe in the Raman spectra, although a signature of the corresponding modes might be identified both in the LT and RT spectra at about 310 cm^{-1} ; the corresponding eigenvectors are shown in Figs. 6(d) and 6(e), respectively. The first mode is a rotation of the Si trimer below Sn (with some substrate participation), while the second mainly enhances the buckling of the topmost Si bilayer.

Above, a distinct peak at 331.9 cm^{-1} is observed experimentally for parallel polarization (A mode). The corresponding displacement pattern is shown in Fig. 6(f): it represents a symmetric movement of the Si trimer below Sn along the Sn-Si bond direction, with some substrate participation.

Two features predicted by theory at 347.3 and 352.7 cm^{-1} appear with low intensity in the measurements. They originate from atomic movements in the topmost Si bilayer. The first one is due to the symmetric movement of three down Si atoms toward one up Si atom, similarly to Fig. 6(f), which indeed has similar energy. The second is a rigid rotation of the Si trimer below Sn, involving to some extent the neighboring atoms, similarly to the pattern displayed in Fig. 6(d).

The two following modes (measured at 385.5 and 416.5 cm^{-1}) in the $z(xx)\bar{z}$ spectrum are believed to be almost independent of the adsorbate atom species, because similar peaks were also observed for other surface reconstructions with Au adatoms. For Au- $(\sqrt{3}\times\sqrt{3})$ /Si(111), peaks at 401 and 419 cm^{-1} with A symmetry, which are mainly located at the Si(111) substrate, were observed at comparable temperatures [40]. The first mode is indeed the symmetric movement of the Si trimer towards Sn illustrated in Fig. 6(f). This mode also exists in the Au/Si(111) system, which also features Si trimers. It has a higher frequency than the mode measured at about 331 cm^{-1} , as the former is characterized by a larger substrate participation and has thus a higher effective mass. The second mode is a vertical displacement of the Si atoms at T_4 positions not covered by Sn, as shown in Fig. 6(g).

The peak experimentally observed at 450.5 cm^{-1} in the Sn/Si(111) spectra lies in the steep edge of the 2TA [62], and is due to an asymmetric movement of the topmost Si trilayer leading to the distortion of the Si trimer below Sn, as schematically displayed in Fig. 6(h).

Similar to Ge(111)- $c(2\times 8)$ and Sn/Ge(111) (see below), Sn/Si(111) also shows a peak on the low-frequency edge of the LTO bulk peak. Here its frequency is measured at LT at 487.5 cm^{-1} . This phonon is completely localized at the topmost Si bilayer and leads to a lateral shearing movements in the (111) plane of the up and down Si atoms, as in Fig. 6(i).

A further peak is predicted by theory at 505.0 cm^{-1} , corresponding to a vertical vibration of the Si dimer below Sn. It is in principle similar to the mode in Fig. 6(g), however it is somewhat blue shifted, due to lower effective mass (two Si dimers swing in the previous mode and only one here) and to the presence of the Sn atoms, which limits the movement of the upper Si atom. In experiments, this frequency is overlapped by the flank of the Si bulk LTO mode and is thus hard to be detected.

The excellent agreement (both in frequency and symmetry) of calculated and measured modes reciprocally validates the theoretical and experimental approach, which seems to be well suited to explore the investigated system.

Beside the complete mode assignment, the Raman spectra also allow the conclusion that the vibration dynamics of Sn/Si(111) shows no indication of a temperature-induced phase transition, in full agreement with STM results [13].

D. High-frequency vibration modes of Sn/Ge(111)

Analogous to Sn/Si(111), also for Ge(111) a new reconstruction is established upon adsorption of 1/3 ML of Sn.

As confirmed by LEED and STM results, the reconstruction of Sn/Ge(111) at RT has many similarities with the previously discussed Sn/Si(111) surface, whose atomic structure is depicted in Fig. 1. As mentioned above, the DF model yields similar results for both, Sn/Ge(111) and Sn/Si(111), for RT.

The (3×3) reconstruction of Sn/Ge(111) belongs to the two-dimensional surface space group $p3m1$, corresponding to the three-dimensional point group C_{3v} . The averaged $(\sqrt{3}\times\sqrt{3})$ reconstruction with equal Sn atoms of Sn/Ge(111) as well as Sn/Si(111) pertains to the group $p31m$, also associated with the group C_{3v} [61]. Hence, all considered adsorbate surface reconstructions obey the same symmetry properties discussed in the previous section, leading to Raman-active A-like and E-like vibration modes.

For time-averaging measurement methods, like conventional LEED and STM, the reconstruction at RT appears to be $(\sqrt{3}\times\sqrt{3})$, in spite of the vertical Sn oscillations according to the DF model. In contrast, the Raman process takes an instantaneous snapshot of the surface [63]. Having this in mind, it is plausible to expect that reconstructions above and below T_{SPT} have similar Raman spectra. An analogous situation is reported for the electronic structure of both Sn/Ge(111) reconstructions measured by photoemission spectroscopy [33].

The surface Raman spectra of Sn/Ge(111) are shown in Fig. 7 for RT and LT. The $c(2\times 8)$ -reconstruction-induced peaks of Fig. 3 have vanished. Instead new peaks appear, which are attributed to the adsorbate-induced reconstruction. Since Ge has a higher atomic mass than Si, it is expected that the eigenfrequencies for Sn-Ge vibration modes are in general lower than for Sn-Si. The somewhat weaker Ge-Ge bond (see Fig. 4) will enhance this effect. Interestingly, although some Raman features appear in similar form in both Sn-Si and Sn-Ge spectra, there is no one-on-one correspondence of the Raman features of Sn/Si(111) and Sn/Ge(111). This is probably due to the much higher Ge atomic mass, which shifts the relative positions of Sn-related and Si(Ge)-related peaks, and affects the degree of localization of the phonon eigenvectors at the surface. Indeed, more surface localized peaks are both detected by Raman spectroscopy and predicted by calculations in the Sn/Ge(111) than in the Sn/Si(111) system. Although a higher number of Raman peaks occurs in a narrower frequency range than in the case of the Sn/Si(111) system, an assignment of the measured features to the calculated phonon modes based on eigenfrequency, symmetry, and comparison with the Sn/Si(111) spectrum is successfully accomplishable.

In the LT spectra, a prominent and narrow peak is located at 105.0 cm^{-1} , which is observed in both polarization

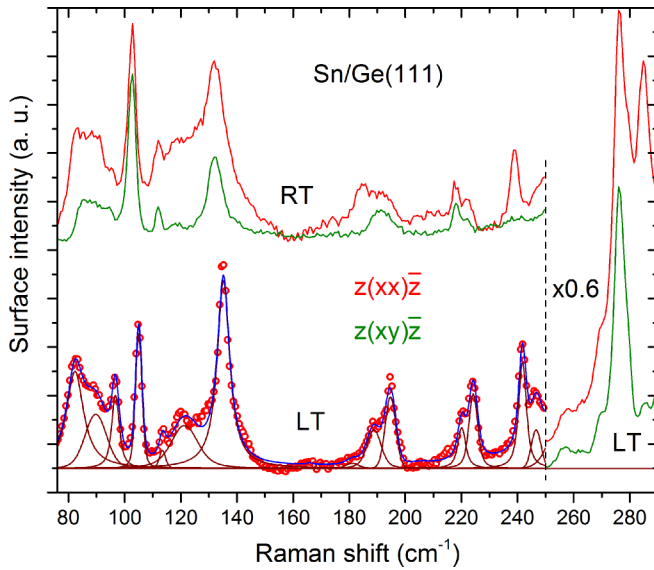


FIG. 7. Surface Raman spectra of the Sn/Ge(111) surface at room temperature (RT) for both polarization configurations and at low temperature (LT, ≈ 40 K) for $z(xx)\bar{z}$ polarization configuration. In the LT spectrum a fit with Voigt profiles is added to illustrate the decomposition of the peaks. The frequency range below 80 cm^{-1} is shown and discussed in more detail in Sec. III E.

configurations. This peak corresponds to the peak at 183.4 cm^{-1} in the Sn/Si(111) system, and its theoretical counterpart is predicted at 97.0 cm^{-1} . The corresponding eigenvector is shown in Fig. 6(b).

On the low-frequency as well as on the high-frequency side of this strong peak there are groups of three peaks. On the low-frequency side the peaks at 82.3 , 89.7 , and 96.8 cm^{-1} are predicted in theory at 80.5 , 82.8 , and 105.3 cm^{-1} . They all correspond to distinct vertical displacements of the Ge dimers at the T_4 positions, in phase or antiphase and with and without Sn participation (see Fig. 8). Also in the case of Sn/Si(111) the shoulder on the left side of the peak at 185.5 cm^{-1} was assigned to a phonon with related displacement pattern.

On the high-frequency side, three phonon modes can be discriminated at 113.5 , 121.4 , and 135.2 cm^{-1} . These peaks are resolved best in the $z(xy)\bar{z}$ configuration, as shown in the RT spectra. Also in DFT-LDA three modes appear in this frequency range at 97.0 , 108.6 , and 131.9 cm^{-1} . However, the symmetry of two of them is not in agreement with the

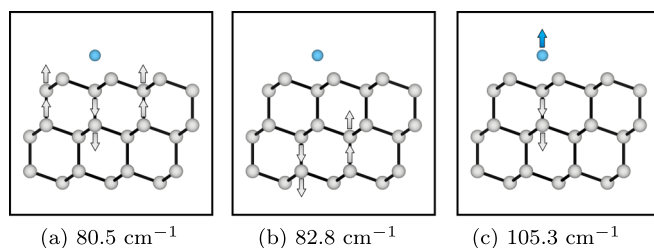


FIG. 8. Calculated displacement patterns of selected surface localized phonon modes in the Sn- $(\sqrt{3}\times\sqrt{3})$ /Ge(111) system. The arrows show the atomic displacement within the $(\sqrt{3}\times\sqrt{3})$ surface unit cell.

experiment. This might be related to spurious polarization components in the $z(xy)\bar{z}$ scattering geometry. The last peak at 131.9 cm^{-1} is a vertical displacement of the Sn atom which has no counterpart in the Sn/Si(111) system.

Our calculations predict two surface phonons at 171.0 and 180.9 cm^{-1} , which are hard to detect in experiment due to the presence of the bulk 2TA phonon structure at 163 cm^{-1} . Beyond the 2TA, there are three double groups of peaks. The peaks are observed at 188.8 , 194.7 , 220.1 , 224.2 , 241.8 , and 246.6 cm^{-1} . Corresponding surface modes are also predicted in theory at 190.4 , 194.2 , 200.4 , 213.7 , and 221.6 cm^{-1} . However, the central doublet has the A symmetry in theory and E in experiment.

Similarly as in the case of Ge(111)-c(2 \times 8), there are peaks on the low-frequency side of the bulk LTO phonon (256.8 , 276.5 , and 285.4 cm^{-1}). The origin might be similar. All these peaks are closely reproduced by the atomistic calculations, which show that the modes detected at the low-frequency side of the bulk LTO phonon are of similar nature in Sn/Ge(111) and Sn/Si(111). The modes predicted at 245.8 , 264.2 , and 296.2 cm^{-1} correspond exactly to the high energy modes of Sn/Si(111) represented in Figs. 6(g), 6(i) and 6(j). All measured Raman peaks are reproduced by the simulations. The mean deviation from the experimental results at RT (LT) amounts to 5.3 (5.8) cm^{-1} .

A comparison of the RT and LT spectra reveals shifts of the peak frequency. The reason for these shifts are anharmonic effects, becoming relevant at higher temperatures. In the spectral region above $\approx 80\text{ cm}^{-1}$, we see no indications for a phase transitions. The peak frequencies for both temperatures are summarized in Table IV.

The Raman spectra of Sn/Si(111) and Sn/Ge(111) feature many modes with the same origin and character. This is strikingly confirmed, e.g., by the RT-frequency ratio of the distinct peaks at 183.4 cm^{-1} of Sn/Si(111) and 102.6 cm^{-1} of Sn/Ge(111). This ratio matches quite well the corresponding value for the bulk LTO phonon of Si and Ge. This indicates that the Sn atoms affect this mode only weakly. Indeed, our calculations reveal that both modes share the same eigenvector, in which the Si(Ge) trimer seesaws about the Sn atom, which is not directly involved in this phonon.

E. Low-frequency vibration modes of Sn/Ge(111) and Sn/Si(111)

In this section, we analyze the Raman signatures of the low-frequency vibration modes of Sn/Ge(111) and Sn/Si(111) and compare them among both materials and with the calculated values. This frequency range includes the vibrations that play a crucial role for the surface fluctuations and the possible occurrence of the $(\sqrt{3}\times\sqrt{3}) \leftrightarrow (3\times 3)$ phase transition.

The relevant frequency region for Sn/Ge(111) is shown for RT and LT and both polarization configurations in Fig. 9. The main peak occurs at 55.6 cm^{-1} for RT and is only marginally upshifted to 55.8 cm^{-1} for LT. This eigenfrequency has been previously associated with the DF mode. It has been identified from HAS experiments as a surface eigenmode in which the displacement vectors of all Sn atoms are pointing vertically in phase, and which has only small admixtures of other modes [29,64]. Two lower surface phonon branches with different

TABLE IV. Vibration peak frequencies (in cm^{-1}) of Sn/Ge(111) above $\approx 80 \text{ cm}^{-1}$ measured by Surface Raman spectroscopy (SRS) in $z(xx)\bar{z}$ polarization configuration. Data are presented for room temperature (RT) and low temperature (LT, $\approx 40 \text{ K}$) and compared with values calculated within DFT-LDA.

Sym.	SRS		DFT	
	RT	LT	Sym.	LDA
A	82.1	82.3	A	80.5
E	88.3	89.7	E	82.8
E	95.8	96.8	A	105.3
E	102.6	105.0	E	97.0
E	111.9	113.5	A	108.6
E	119.2	121.4	E	131.9
E	132.4	135.2	A	138.7
A		165.9	A	171.0
A		181.1	A	180.9
A	184.8	188.8	A	190.4
E	192.5	194.7	E	194.2
A		205.4	A	200.4
E	217.8	220.1	A	213.7
E	222.4	224.2	A	221.6
A	238.8	241.8	A	242.9
A		246.6	A	248.3
E	254.1	256.8	E	245.8
E		270.0	E	264.2
E	271.1	276.5	E	268.2
A	280.7	285.4	A	296.2

eigenvectors, which were also reported from HAS data [29], are below the accessible frequency range of SRS. In HAS measurements, a signal with low intensity at $\approx 71 \text{ cm}^{-1}$ was found and attributed to backfolded RWs [41], but could not be observed in the Raman spectra, maybe due to its weak Raman scattering efficiency.

In regard to the assignment of the main peak at 55.8 cm^{-1} in Fig. 9, it should be noted that this very pronounced feature is observed with equal intensity for both polarization configurations. This behavior distinctly points to a vibration mode with E-symmetry character. This is in contrast to the symmetry of the vertical displacement of the Sn atoms, which has A character. The feasibility of allocating an E mode to the main peak is underscored by our calculations. They predict an E-type surface vibration mode at 55.3 cm^{-1} , i.e., a nearly perfect frequency match. The calculated mode represents a lateral displacement of the Sn atom, with corresponding tilting of the subjacent Ge trimer, as shown in Fig. 10(a).

While the (3×3) -periodic phase of the Sn/Si(111) surface is not stable, the (3×3) -periodic phase of the Sn/Ge(111) surface represents the energy ground state of this system. Thus, in order to achieve a complete theoretical description of the Sn/Ge(111) surface, we also performed frozen-phonon calculations for the (3×3) reconstruction. For this geometry three additional modes of A symmetry appear, which are based on the above mentioned vertical displacements of the Sn atoms, as shown in Fig. 11. Furthermore they involve (minor) displacements in the first Ge double layer (not shown). For two of these modes [Figs. 11(a) and 11(b)] the predicted

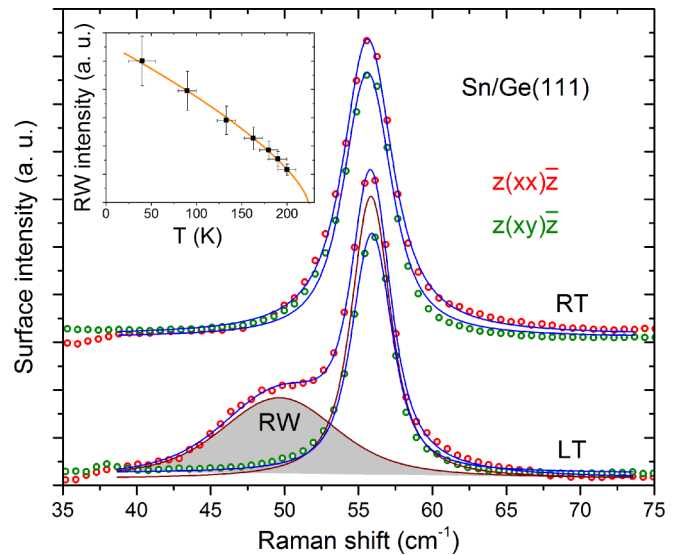


FIG. 9. Low-frequency surface Raman spectra of Sn/Ge(111) at room temperature (RT) and low temperature (LT, $\approx 40 \text{ K}$). Both polarization configurations are shown. The emerging shoulder (shaded area) on the low-frequency side of the main peak at LT is identified with a backfolded Rayleigh wave (RW) and acts as an indication for the structural phase transition. The inset shows the RW intensity development with temperature.

frequencies are about 47 cm^{-1} , i.e., rather close to the frequency which in literature has been assigned to the DF mode [29]. These Sn displacement patterns closely resemble two of the three eigenvectors identified by Farias *et al.* as a basis set for the description of the reaction coordinate leading from the $(\sqrt{3} \times \sqrt{3})$ to the (3×3) periodicity [64].

The third mode of the basis set, shown in Fig. 11(c), is predicted by our calculations at a significantly higher frequency than the other two. This is due to the fact that this mode affects to a lesser extent the Ge substrate, resulting in a much lower effective mass.

According to previous calculations, the frequency of the DF mode declines to zero with decreasing temperature for Sn/Ge(111) at the \bar{K} point of the surface BZ, in conjunction with the structural phase transition [24]. The direct observation of this softening is not possible in SRS due to

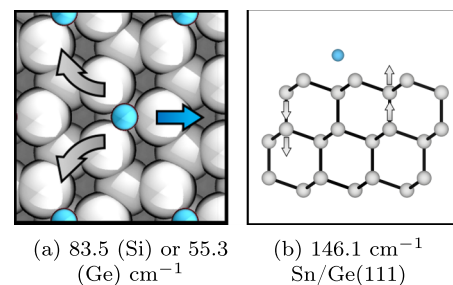


FIG. 10. Calculated displacement pattern and eigenfrequency of selected surface localized phonon modes in the Sn- $(\sqrt{3} \times \sqrt{3})$ /Si(Ge)(111) system. The arrows show the atomic displacement within the $(\sqrt{3} \times \sqrt{3})$ surface unit cell. Rounded arrows represent the seesaw movement of the Si(Ge) trimer below the Sn atom.

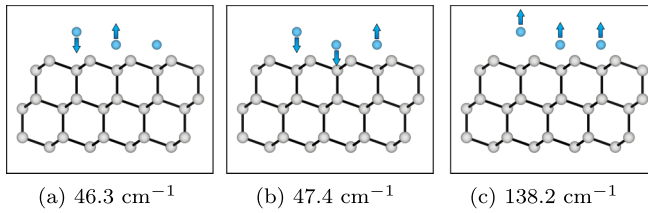


FIG. 11. Schematic representation of the calculated eigenmodes of the Sn-(3×3)/Ge(111) system, which are related to the dynamic fluctuation. The arrows show the atomic displacement within the (3×3) surface unit cell.

the confinement of this method to the center of the BZ, i.e., only vibration modes close to the $\bar{\Gamma}$ point can be detected by first-order SRS. Yet, the temperature-dependent Raman spectra contain a direct signature of the phase transition, which is discussed next.

Figure 9 shows that upon cooling below T_{SPT} next to the main peak a low-frequency shoulder appears which is centered at 49.6 cm^{-1} . This emerging feature is attributed to the backfolding of a RW, whose frequency at the \bar{K} point was determined to $\approx 50 \text{ cm}^{-1}$ by HAS [41]. Due to the backfolding, the \bar{K} point of the $(\sqrt{3} \times \sqrt{3})$ surface BZ becomes the new $\bar{\Gamma}$ point of the (3×3) reconstruction. Because of its localization at the surface, the RW is intrinsically sensitive to changes in the surface reconstruction [59]. Therefore, we assess the emergence of the shoulder as a signature of the structural phase transition of Sn/Ge(111), whose quantitative analysis yields further information about this transition.

The intensity development of the backfolded-RW peak versus temperature is shown in the inset of Fig. 9. Obviously, the RW intensity strongly increases with decreasing temperature. A power law is fitted as a guide to the eye, suggesting a transition temperature of $\approx 225 \text{ K}$, which matches well with the reported values for T_{SPT} [12,14]. Our interpretation of the intensity development is as follows. Above T_{SPT} , all Sn atoms fluctuate randomly on a short time scale. Cooling the sample to T_{SPT} initializes a freeze-out of these fluctuations, at first in incoherent patches. Upon further cooling, the residual fluctuation probability is reduced, resulting in larger patches of an ordered (3×3) reconstruction with larger coherence length, which leads to the increase of the backfolded RW in the Raman spectrum. Hence, the Raman measurements point to a phase transition of the order-disorder type. This is in agreement with literature [14,29,65], although a transition of the displacive type is usual for systems hosting soft phonons.

The spectra of Sn/Ge(111) presented so far support the assessment that the $(\sqrt{3} \times \sqrt{3})$ and (3×3) reconstructions are very similar, when measured by SRS. The only significant change is the appearance of the backfolded RW, which is the result of coherence of adjacent surface unit cells. All other modes are not influenced by structural changes. All frequency values are summarized in Table V together with DFT calculations and previous theoretical and HAS results for comparison.

The low-frequency Raman spectra for Sn/Si(111) are shown for both polarization configurations in Fig. 12. The peak at 88.3 cm^{-1} is the counterpart for the main peak of Sn/Ge(111) in Fig. 10. All values of Sn/Si(111) are also

TABLE V. Vibration peak frequencies (in cm^{-1}) of the low-frequency peaks for Sn/Ge(111) and Sn/Si(111) in $z(xx)\bar{z}$ polarization configuration. Data measured by surface Raman spectroscopy (SRS) are presented for room temperature (RT) and low temperature (LT, $\approx 40 \text{ K}$) together with the density functional theory (DFT) calculations of this work. Further results of He atom scattering (HAS) [29,41] are given for comparison. The HAS data are given for 145 K.

	SRS		Symm. ($\sqrt{3} \times \sqrt{3}$)	DFT	
	RT	LT		LT	HAS
Sn/Ge			E	15.4	22
			E	36.8	34
		49.6	A	37.9	50
	55.6	55.8	E	55.3	55
			A	76.8	72
Sn/Si			A	25.5	
	58.0	58.0	A	58.7	
	85.9	88.3	E	83.5	
	118.0	121.0	A	138.7	

summarized in Table V. In contrast to Sn/Ge(111), the main peak is shifted with temperature by 2.4 cm^{-1} . Here, we see a clear distinction between the modes of the different systems and a possible hint to their different LT behavior. This discrepancy between Sn/Ge(111) and Sn/Si(111) could be a starting point to evaluate the phase transition regarding the absence of anharmonic terms for Sn/Ge(111) to electronic correlations.

Apart from the main peak, there is an additional structure at 118.0 cm^{-1} (marked by an arrow in Fig. 12), which is only observed in parallel polarization configuration and declines at LT. A possible origin for this peak is a second-order process involving the \bar{K} and \bar{M} points of the surface BZ,

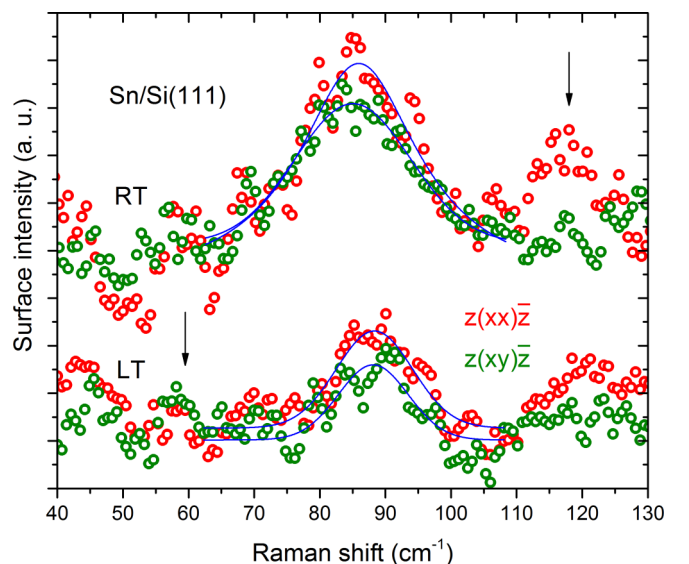


FIG. 12. Surface Raman spectra of Sn/Si(111) in the low frequency spectral range at room temperature (RT) and low temperature (LT, $\approx 40 \text{ K}$). Both polarization configurations are shown.

where the density of states is elevated due to the flat phonon dispersion [24].

The calculations performed for the Sn/Si(111) with the $(\sqrt{3}\times\sqrt{3})$ periodicity reproduce in this case all measured Raman signatures. Besides a mode of E symmetry at 25.4 cm^{-1} , which represents a lateral shearing of the Sn ML with respect to the Si substrate, but which is experimentally not accessible due to its low frequency, a mode at 58.7 cm^{-1} is predicted, corresponding to the mode at 37.9 cm^{-1} of the Sn/Ge system. This mode is a vertical breathing of the whole surface. At 83.5 cm^{-1} , i.e., roughly the frequency of the main peak, we calculate a mode of E symmetry corresponding to the Sn lateral movement shown in Fig. 10(a) and also predicted for the Sn/Ge system at 55.3 cm^{-1} . Finally, a mode appears at approximately 138.7 cm^{-1} , whose frequency interestingly is identical for the Sn/Si(111) and Sn/Ge(111) system, because this vibration corresponds to the upward movement of the Sn atom without involvement of the substrate atoms. A further phonon with eigenvector shown in Fig. 10(b) occurs at 146.1 cm^{-1} for the Sn- $(\sqrt{3}\times\sqrt{3})$ /Ge(111) system, i.e., in the spectral region between the one presented in Fig. 7 and the one shown in Fig. 12.

IV. SUMMARY

Temperature- and polarization-dependent Raman spectra were recorded for the Sn-induced surface reconstructions on Ge(111) and Si(111). Corresponding calculations of the surface vibration eigenmode frequencies and displacement patterns based on the density functional theory were performed to provide an interpretation of the experimental findings. For Sn/Ge(111), the reversible structural phase transition from $(\sqrt{3}\times\sqrt{3})$ to (3×3) is observed upon cooling. The

transformation is connected to the appearance of a backfolded Rayleigh wave in the low-frequency Raman spectrum. An analogous mode for Sn/Si(111) does not occur. The intensity development of the backfolded Rayleigh wave in Sn/Ge(111) yields a phase transition temperature close to the reported one of $T_{\text{SPT}} \approx 210\text{--}220\text{ K}$. As a key result of our investigation, we deduce from the temperature dependence of the folded-mode intensity that the phase transition is of order-disorder type due to forming of coherent (3×3) patches, whose coherence length grows with decreasing temperature. After freeze-out, these patches do not participate in the dynamical fluctuations. Furthermore, for both adsorbate systems, Sn/Ge(111) and Sn/Si(111), a large group of surface vibration modes was determined with high frequency accuracy in the Raman spectra for room temperature and low temperature ($\approx 40\text{ K}$) in the spectral range up to the bulk optical phonon. These modes show no phase transition signatures. The vibration mode eigenfrequencies determined by surface Raman spectroscopy are in very good agreement with our theoretical calculations, which have allowed the assignment of the vibration patterns and symmetry properties to the modes observed in this work.

ACKNOWLEDGMENTS

We gratefully acknowledge financial support by the Deutsche Forschungsgemeinschaft in the research units FOR1162 (Project GE 1855/10-2), FOR1700 (Project SA 1948/1-2), and FOR2824 (Project SA 1948/2-1). The Höchstleistungsrechenzentrum Stuttgart (HLRS) is gratefully acknowledged for grants of high-performance computer time. We also acknowledge computational resources provided by the HPC Core Facility and the HRZ of the Justus-Liebig-Universität Gießen.

-
- [1] D. J. Chadi and C. Chiang, *Phys. Rev. B* **23**, 1843 (1981).
 - [2] R. E. Schlier and H. E. Farnsworth, *J. Chem. Phys.* **30**, 917 (1959).
 - [3] F. Flores, J. Ortega, and R. Pérez, *Surf. Rev. Lett.* **06**, 411 (1999).
 - [4] O. Pulci, P. Gori, M. Marsili, V. Garbuio, A. P. Seitsonen, F. Bechstedt, A. Cricenti, and R. Del Sole, *Phys. Status Solidi (a)* **207**, 291 (2010).
 - [5] R. S. Becker, J. A. Golovchenko, and B. S. Swartzentruber, *Phys. Rev. Lett.* **54**, 2678 (1985).
 - [6] R. S. Becker, B. S. Swartzentruber, J. S. Vickers, and T. Klitsner, *Phys. Rev. B* **39**, 1633 (1989).
 - [7] N. Takeuchi, A. Selloni, and E. Tosatti, *Phys. Rev. B* **51**, 10844 (1995).
 - [8] P. Molinàs-Mata and J. Zegenhagen, *Solid State Commun.* **84**, 393 (1992).
 - [9] N. Takeuchi, A. Selloni, and E. Tosatti, *Phys. Rev. Lett.* **69**, 648 (1992).
 - [10] J. Lobo, D. Fariás, E. Hulpke, J. P. Toennies, and E. G. Michel, *Phys. Rev. B* **74**, 035303 (2006).
 - [11] O. Bunk, J. H. Zeysing, G. Falkenberg, R. L. Johnson, M. Nielsen, M. M. Nielsen, and R. Feidenhans'l, *Phys. Rev. Lett.* **83**, 2226 (1999).
 - [12] J. M. Carpinelli, H. H. Weitering, M. Bartkowiak, R. Stumpf, and E. W. Plummer, *Phys. Rev. Lett.* **79**, 2859 (1997).
 - [13] H. Morikawa, I. Matsuda, and S. Hasegawa, *Phys. Rev. B* **65**, 201308(R) (2002).
 - [14] L. Floreano, D. Cvetko, G. Bavdek, M. Benes, and A. Morgante, *Phys. Rev. B* **64**, 075405 (2001).
 - [15] S. Modesti, L. Petaccia, G. Ceballos, I. Vobornik, G. Panaccione, G. Rossi, L. Ottaviano, R. Larciprete, S. Lizzit, and A. Goldoni, *Phys. Rev. Lett.* **98**, 126401 (2007).
 - [16] R. Cortés, A. Tejada, J. Lobo, C. Didiot, B. Kierren, D. Malterre, E. G. Michel, and A. Mascaraque, *Phys. Rev. Lett.* **96**, 126103 (2006).
 - [17] G. Profeta and E. Tosatti, *Phys. Rev. Lett.* **98**, 086401 (2007).
 - [18] G. Li, P. Höpfner, J. Schäfer, C. Blumenstein, S. Meyer, A. Bostwick, E. Rotenberg, R. Claessen, and W. Hanke, *Nat. Commun.* **4**, 1620 (2013).
 - [19] A. Goldoni and S. Modesti, *Phys. Rev. Lett.* **79**, 3266 (1997).
 - [20] T. E. Kidd, T. Miller, and T.-C. Chiang, *Phys. Rev. Lett.* **83**, 2789 (1999).
 - [21] A. V. Melechko, J. Braun, H. H. Weitering, and E. W. Plummer, *Phys. Rev. B* **61**, 2235 (2000).
 - [22] L. Petersen, Ismail, and E. W. Plummer, *Phys. Rev. B* **65**, 020101(R) (2001).

- [23] J. Avila, A. Mascaraque, E. G. Michel, M. C. Asensio, G. Le Lay, J. Ortega, R. Pérez, and F. Flores, *Phys. Rev. Lett.* **82**, 442 (1999).
- [24] R. Pérez, J. Ortega, and F. Flores, *Phys. Rev. Lett.* **86**, 4891 (2001).
- [25] M. E. Dávila, J. Avila, M. C. Asensio, and G. Le Lay, *Surf. Rev. Lett.* **10**, 981 (2003).
- [26] F. Ronci, S. Colonna, S. D. Thorpe, A. Cricenti, and G. Le Lay, *Phys. Rev. Lett.* **95**, 156101 (2005).
- [27] J. S. Okasinski, C.-Y. Kim, D. A. Walko, and M. J. Bedzyk, *Phys. Rev. B* **69**, 041401(R) (2004).
- [28] L. Petaccia, L. Floreano, M. Benes, D. Cvetko, A. Goldoni, L. Grill, A. Morgante, A. Verdini, and S. Modesti, *Phys. Rev. B* **63**, 115406 (2001).
- [29] D. Farías, W. Kamiński, J. Lobo, J. Ortega, E. Hulpke, R. Pérez, F. Flores, and E. G. Michel, *Phys. Rev. Lett.* **91**, 016103 (2003).
- [30] J. Ortega, R. Pérez, and F. Flores, *J. Phys.: Condens. Matter* **14**, 5979 (2002).
- [31] A. A. Escuadro, D. M. Goodner, J. S. Okasinski, and M. J. Bedzyk, *Phys. Rev. B* **70**, 235416 (2004).
- [32] F. Ronci, S. Colonna, A. Cricenti, and G. Le Lay, *Phys. Rev. Lett.* **99**, 166103 (2007).
- [33] J. Ortega, R. Pérez, and F. Flores, *J. Phys.: Condens. Matter* **12**, L21 (2000).
- [34] S. Sakong, P. Kratzer, S. Wall, A. Kalus, and M. Horn-von Hoegen, *Phys. Rev. B* **88**, 115419 (2013).
- [35] E. Speiser, N. Esser, S. Wippermann, and W. G. Schmidt, *Phys. Rev. B* **94**, 075417 (2016).
- [36] M. Liebhaber, B. Halbig, U. Bass, J. Geurts, S. Neufeld, S. Sanna, W. G. Schmidt, E. Speiser, J. Räthel, S. Chandola, and N. Esser, *Phys. Rev. B* **94**, 235304 (2016).
- [37] G. Benedek, I. Sklyadneva, E. Chulkov, P. Echenique, R. Heid, K.-P. Bohnen, D. Schmicker, S. Schmidt, and J. Toennies, *Surface Sci.* **678**, 38 (2018).
- [38] J. Räthel, E. Speiser, N. Esser, U. Bass, S. Meyer, J. Schäfer, and J. Geurts, *Phys. Rev. B* **86**, 035312 (2012).
- [39] M. Liebhaber, U. Bass, P. Bayersdorfer, J. Geurts, E. Speiser, J. Räthel, A. Baumann, S. Chandola, and N. Esser, *Phys. Rev. B* **89**, 045313 (2014).
- [40] B. Halbig, M. Liebhaber, U. Bass, J. Geurts, E. Speiser, J. Räthel, S. Chandola, N. Esser, M. Krenz, S. Neufeld, W. G. Schmidt, and S. Sanna, *Phys. Rev. B* **97**, 035412 (2018).
- [41] J. Lobo, D. Farías, E. Hulpke, and E. G. Michel, *Phys. Rev. B* **71**, 205402 (2005).
- [42] T. C. Damen, S. P. S. Porto, and B. Tell, *Phys. Rev.* **142**, 570 (1966).
- [43] *Light Scattering in Solids II: Basic Concepts and Instrumentation*, edited by M. Cardona and G. Güntherodt, Topics in Applied Physics Vol. 50 (Springer Verlag, Berlin, Heidelberg, 1982).
- [44] J. Neugebauer and M. Scheffler, *Phys. Rev. B* **46**, 16067 (1992).
- [45] L. Bengtsson, *Phys. Rev. B* **59**, 12301 (1999).
- [46] G. Kresse and J. Furthmüller, *Comput. Mater. Sci.* **6**, 15 (1996).
- [47] G. Kresse and J. Furthmüller, *Phys. Rev. B* **54**, 11169 (1996).
- [48] G. P. Srivastava, *The Physics of Phonons* (CRC Press, Boca Raton, US, 1990).
- [49] W. Kohn and L. J. Sham, *Phys. Rev.* **140**, A1133 (1965).
- [50] D. M. Ceperley and B. J. Alder, *Phys. Rev. Lett.* **45**, 566 (1980).
- [51] J. P. Perdew, J. A. Chevary, S. H. Vosko, K. A. Jackson, M. R. Pederson, D. J. Singh, and C. Fiolhais, *Phys. Rev. B* **46**, 6671 (1992).
- [52] J. P. Perdew, K. Burke, and M. Ernzerhof, *Phys. Rev. Lett.* **77**, 3865 (1996).
- [53] P. E. Blöchl, *Phys. Rev. B* **50**, 17953 (1994).
- [54] G. Kresse and D. Joubert, *Phys. Rev. B* **59**, 1758 (1999).
- [55] H. J. Monkhorst and J. D. Pack, *Phys. Rev. B* **13**, 5188 (1976).
- [56] B. A. Weinstein and M. Cardona, *Phys. Rev. B* **7**, 2545 (1973).
- [57] L. Dobrzynski and D. Mills, *J. Phys. Chem. Solids* **30**, 1043 (1969).
- [58] L. Dobrzynski and D. L. Mills, *Phys. Rev. B* **7**, 1322 (1973).
- [59] F. Bechstedt, *Principles of Surface Physics* (Springer Verlag, Berlin, Heidelberg, 2003).
- [60] Radii of atoms and ions, www.webelements.com (2019), accessed online on 17 April, 2019.
- [61] A. Cano, A. P. Levanyuk, and E. G. Michel, *Nanotechnology* **16**, 325 (2005).
- [62] K. Uchinokura, T. Sekine, and E. Matsuura, *J. Phys. Chem. Solids* **35**, 171 (1974).
- [63] *Light Scattering in Solids I: Introductory Concepts*, edited by M. Cardona, Topics in Applied Physics Vol. 8 (Springer Verlag, Berlin, Heidelberg, 1975).
- [64] D. Farías, W. Kamiński, J. Lobo, J. Ortega, E. Hulpke, R. Pérez, F. Flores, and E. G. Michel, *Appl. Surf. Sci.* **237**, 86 (2004).
- [65] L. Petaccia, L. Floreano, A. Goldoni, D. Cvetko, A. Morgante, L. Grill, A. Verdini, G. Comelli, G. Paolucci, and S. Modesti, *Phys. Rev. B* **64**, 193410 (2001).